Structural diversity in hybrid lead halides templated by 4-methylimidazolium

Clement Elliott,[1] Jason A. McNulty,[1] David B. Cordes,[1] Alexandra M. Z. Slawin[1] and Philip Lightfoot[1]*

[1]EaStCHEM, School of Chemistry, University of St Andrews, St Andrews, KY16 9ST, United Kingdom

*pl@st-andrews.ac.uk

Abstract:

We present several new hybrid organic-inorganic lead(II) bromide materials with interesting polyhedral connectivity templated by [4-MeImH] ([4-MeImH] = 4-methylimidazolium). These include two new examples of a 1D structure-type consisting of edge-sharing chains ([4-MeImH]PbBr$_3$ and [4-MeImH]$_{0.6}$[ImH]$_{0.4}$PbBr$_3$, [ImH] = imidazolium); the first example of a 2D layered material containing 7-coordinate Pb, and featuring edge- and face-sharing polyhedra ([4-MeImH]Pb$_2$Br$_5$) and two examples of materials consisting of corner- and face-sharing octahedra; [ImH]PbBr$_3$, which has a 4H-perovskite structure and [4-MeImH]$_4$[ImH]$_5$Pb$_6$Br$_{21}$, which has a structural resemblance to the 4H-perovskite, but incorporates terminal Br ligands leading to a complex layered structure.

Keywords: Single crystal X-ray diffraction; Lead halides; Polyhedral connectivity; Structure-directing effects; Hybrid Organic-Inorganic.

1. Introduction

Organic-inorganic hybrid materials have undergone significant study in recent times due to their compositional and structural flexibility and the tuneable physical and chemical properties arising from this.[1–3] Recently, many of these studies have moved away from the archetypal 3D-perovskite structure, ABX$_3$, and instead are targeting lower dimensional structures in an effort to design materials with desirable physical properties, such as photoluminescence.[4–6] Some examples of materials with reduced dimensionality are (100)-oriented[7,8] and (110)-oriented[9–11] perovskites and layered B-site deficient 'hollow' perovskites.[12] All three of these structure-types consist of a corner-linked inorganic octahedral framework that has been either 'sliced' [as in both (100)- and (110)-oriented structures] or features compositional deficiency (B-site deficient 'hollow' perovskites) resulting in a disruption of the repeating 3D framework. Of these structure-types, the (100)-oriented perovskite has undergone considerably more study due to the compositional variability afforded by the interlayer site.[3,13-15] However,

several other related structure-types featuring polyhedral connectivity other than corner-linkages, such as edge- or face-sharing are known. These include the well-known face-sharing hexagonal perovskites[16,17] and the relatively rare edge-sharing chains,[18–22] both of which are 1D frameworks. It is worth noting that variations of hexagonal perovskite can include both face- and corner-sharing polyhedra.

In our previous work,[7,10,11,12] we studied the effect of different disc-shaped monoprotonated amines and reported several examples of materials featuring octahedral connectivity. We have previously shown that the hydrogen-bonding preferences and size of these amines can have a significant effect on structure. An example of this is the use of [1-MeImH] in $[1\text{-MeImH}]_{0.5}[\text{GuH}]_{1.5}\text{SnI}_4$ ([1-MeImH = 1-methylimidazolium and [GuH] = guanidinium) where we have shown that the limitations on hydrogen-bonding arising from the use of the methyl group on the 1-position results in distinct ordering of the organic moieties. We have also recently shown that different derivatives of disc-shaped amines, for example the 1- and 4-isomers of methylimidazolium, can template differing packing architectures of similar inorganic units due to this same optimisation of hydrogen-bonding.[23]

In the present paper, we report several new hybrid lead bromide materials, inspired by our previous work, primarily templated by the disc-shaped monoprotonated amine [4-MeImH] (4-methylimidazolium) or a mixture of [4-MeImH] and imidazolium [ImH]. The present compounds adopt a variety of different structure-types corresponding to different polyhedral connectivity, *viz.* 1D edge-sharing chains for $[4\text{-MeImH}]\text{PbBr}_3$ and $[4\text{-MeImH}]_{0.6}[\text{ImH}]_{0.4}\text{PbBr}_3$, 2D edge- and face-sharing layers for $[4\text{-MeImH}]\text{Pb}_2\text{Br}_5$ and face- and corner-sharing hexagonal perovskite derivatives for $[4\text{-MeImH}]_4[\text{ImH}]_5\text{Pb}_6\text{Br}_{21}$ and $[\text{ImH}]\text{PbBr}_3$.

2. Experimental

2.1. Materials

Lead (II) bromide (PbBr_2, ≥98%), hydrobromic acid (HBr, 48%, w/w aqueous solution), 4-methylimidazole ($\text{C}_4\text{H}_7\text{N}_2$, 98%), imidazole ($\text{C}_3\text{H}_5\text{N}_2$, 99%) and 1-methylimidazole ($\text{C}_4\text{H}_7\text{N}_2$, 98%) were purchased from Alfa Aesar. Diethyl ether (($\text{C}_2\text{H}_5)_2\text{O}$, 99.5%) was purchased from Sigma Aldrich. All chemicals were directly used without further purification. All samples were obtained by slow-evaporation methods.

2.2. Sample Preparation

2.2.1. [4-MeImH]PbBr₃

Stoichiometric amounts of 4-methylimidazole (332 mg, 4 mmol) and PbBr_2 (369 mg, 1 mmol) were dissolved in conc. HBr (2.42 mL) with moderate heating. By cooling for a few hours, colourless needle-shaped crystals of approximate dimensions 0.15 mm × 0.15 mm × 0.4 mm

were obtained. These were filtered and washed with diethyl ether. Elemental analysis: Anal. Calc. (%) for $(C_4N_2H_7)PbBr_3$: C, 9.06; H, 1.33; N, 5.29. Found: C, 9.87; H, 1.44; N, 5.13.

2.2.2. Preparation of [4-MeImH]$_{0.6}$[ImH]$_{0.4}$PbBr$_3$

Stoichiometric amounts of 4-methylimidazole (166 mg, 2 mmol), imidazole (138 mg, 2 mmol) and $PbBr_2$ (737 mg, 2 mmol) were dissolved in conc. HBr (2.6 mL) with moderate heating. By cooling for a few hours, colourless, cuboid-shaped crystals of approximate dimensions 0.05 mm × 0.05 mm × 0.1 mm were obtained. These were filtered and washed with diethyl ether. Elemental analysis: Anal. Calc. (%) for $(C_{3.6}N_2H_{6.2})PbBr_3$: C, 8.25; H, 1.19; N, 5.34. Found: C, 8.24; H, 1.09; N, 5.14.

2.2.3. Preparation of [4-MeImH]$_2$Pb$_2$Br$_5$

Stoichiometric amounts of 4-methylimidazole (166 mg, 2 mmol) and $PbBr_2$ (737 mg, 2 mmol) were dissolved in conc. HBr (2.6 mL) with moderate heating. By cooling for a few hours, colourless needle-shaped crystals were obtained of approximate dimensions 0.01 mm × 0.01 mm × 0.25 mm. These were filtered and washed with diethyl ether. Elemental analysis: Anal. Calc. (%) for $(C_4N_2H_7)Pb_2Br_5$: C, 5.36; H, 0.79; N, 3.12. Found: C, 5.51; H, 0.80; N, 3.38.

2.2.4. Preparation of [ImH]PbBr$_3$ and [4-MeImH]$_4$[ImH]$_5$Pb$_6$Br$_{21}$

Stoichiometric amounts of 4-methylimidazole (83 mg, 1 mmol), imidazole (69 mg, 1 mmol) and $PbBr_2$ (737 mg, 2 mmol) were dissolved in conc. HBr (3 mL) with moderate heating. By cooling for a few hours, a mixture of colourless crystals of approximate dimensions 0.1 mm × 0.1 mm × 0.1 mm were obtained. Some of these crystals were extracted, separated, filtered and washed with diethyl ether. Crystals used in the structure determination of [ImH]PbBr$_3$ were filtered but those used for [4-MeImH]$_4$[ImH]$_5$Pb$_6$Br$_{21}$ were left in solution. Elemental analysis was obtained for these separated crystals: Anal. Calc. (%) for $(C_3N_2H_5)PbBr_3$: C, 6.98; H, 0.98; N, 5.43. Found: C, 7.21; H, 0.74; N, 5.20; Anal. Calc. (%) for $C_{31}N_{18}H_{53}Pb_6Br_{21}$: C, 10.35; H, 1.48; N, 7.01. Found: C, 10.83; H, 1.33; N, 7.07.

2.2. X-ray Crystallography

Single crystal data were collected at 173 K for all samples. Data for all samples except [4-MeImH]PbBr$_3$ were collected using a Rigaku FR-X Ultrahigh Brilliance Microfocus RA generator/confocal optics with XtaLAB P200 diffractometer [Mo Kα radiation (λ = 0.71075 Å)]. Data for [4-MeImH]PbBr$_3$ were collected on a Rigaku SCX Mini CCD diffractometer with a SHINE monochromator (Mo-Kα radiation). Intensity data were collected using ω steps accumulating area detector images spanning at least a hemisphere of reciprocal space. Data were collected using CrystalClear (Rigaku)[24] and processed (including correction for Lorentz, polarization and absorption) using either CrystalClear[24] or CrysAlisPro.[25] Structures were solved by dual-space methods (SHELXT[26]), and refined using SHELX-2018/3[27] incorporated in either the WINGX[28] or Olex2[29] interface. Non-hydrogen atoms were refined anisotropically and hydrogen atoms were treated as riding atoms. Selected crystallographic data are presented in Table 1.

3. Results and Discussion

The crystal data and structure refinement parameters for all compositions are listed in Table 1, with selected bond lengths and angles in Table S2. The newly synthesised materials fall into three structure-types; 1. 1D edge-sharing chains, 2. 2D edge- & face-sharing layers and 3. Face- and corner-sharing hexagonal perovskite derivatives.

3.1 1D edge-sharing chains

Two of the newly synthesised materials, $[4\text{-MeImH}]PbBr_3$ and $[4\text{-MeImH}]_{0.6}[ImH]_{0.4}PbBr_3$, belong to this first group of structures. They have the general formula ABX_3, like cubic perovskite, but consist of $[PbBr_3]_\infty$ edge-sharing chains similar to those found in $\delta\text{-CsPbI}_3$,[30] which can be considered an archetype of this structure (Fig. 1). While both $[4\text{-MeImH}]PbBr_3$ and $[4\text{-MeImH}]_{0.6}[ImH]_{0.4}PbBr_3$ contain [4-MeImH] as a structure-directing agent, [4-MeImH]$_{0.6}[ImH]_{0.4}PbBr_3$ additionally contains the related disc-shaped amine imidazolium, [ImH]. This results in substitutional disorder of the same site in a 60:40 ratio of [4-MeImH] to [ImH]. To the best of our knowledge this is the only known example of a structure of this type featuring this behaviour. While neither $[4\text{-MeImH}]PbBr_3$ or $[4\text{-MeImH}]_{0.6}[ImH]_{0.4}PbBr_3$ have previously been reported, the iodide analogue of $[4\text{-MeImH}]PbBr_3$, $[4\text{-MeImH}]PbI_3$ was previously studied by Guo *et al*.,[18] where the structure was described as consisting of a hexagonal PbX_2 structure that has been stripped of a double strand of condensed PbX_6 octahedra. This results in the short *a*-axis observed in both $[4\text{-MeImH}]PbBr_3$ and $[4\text{-MeImH}]_{0.6}[ImH]_{0.4}PbBr_3$ (4.4308(3) and 4.3643(1) Å, respectively) similar to that observed in $[4\text{-MeImH}]PbI_3$ (4.6110(2) Å) . Unlike $[4\text{-MeImH}]PbI_3$ ($P2_1/c$) both $[4\text{-MeImH}]PbBr_3$ and $[4\text{-MeImH}]_{0.6}[ImH]_{0.4}PbBr_3$ crystallise in the triclinic space group $P\overline{1}$ (with Pb-Br bond distances between 2.960(2) to 3.318(109) and 2.9803(4)-3.2825(7) Å, respectively) with an undoubled *b*-axis and significant differences in the unit cell angles. Comparison of the structural distortions of $[4\text{-MeImH}]PbBr_3$ and $[4\text{-MeImH}]_{0.6}[ImH]_{0.4}PbBr_3$ to $[4\text{-MeImH}]PbI_3$ and δ-CsPbI$_3$ in order to understand the difference in structural behaviour was carried out. The mean distortion level (Δd) and bond angle variance (σ^2) of each octahedron were calculated (details are provided in ESI†), along with those for several related compounds, and the values shown in Table 2. The mean distortion level of both $[4\text{-MeImH}]PbBr_3$ and $[4\text{-MeImH}]_{0.6}[ImH]_{0.4}PbBr_3$ are significantly larger than in either $[4\text{-MeImH}]PbI_3$ or δ-CsPbI$_3$ suggesting that the change in cell structure is likely predominantly due to this. This is further supported by the similarities in calculated BVS for each atom with the general trend that the

terminal halide (X2) is the most severely 'underbonded' and that the bridging halide (X3) is the least 'underbonded'. While there are some significant differences in the bond angle variance between compositions, the exact origin of this remains unclear, however the significant reduction of σ^2 in [4-MeImH]$_{0.6}$[ImH]$_{0.4}$PbBr$_3$ is likely a direct result of the partial incorporation of [ImH], resulting in a smaller structural distortion compared to the larger [4-MeImH] cation.

In both [4-MeImH]PbBr$_3$ and [4-MeImH]$_{0.6}$[ImH]$_{0.4}$PbBr$_3$ the orientation of [4-MeImH] is important in determining where hydrogen bonding is possible. While there are similarities in the orientation of [4-MeImH] in each, there is a subtle change in hydrogen bonding notably at the N1 position (Fig. 1). In [4-MeImH]PbBr$_3$ there are two possible bonds, (N1-H1$\cdots$Br2 3.50 Å and N1-H1$\cdots$Br3 3.42 Å). A slight rotation of the amine in [4-MeImH]$_{0.6}$[ImH]$_{0.4}$PbBr$_3$ compared to [4-MeImH]PbBr$_3$ results in a change from two to one possible H-bond. However, this results in a closer arrangement in [4-MeImH]$_{0.6}$[ImH]$_{0.4}$PbBr$_3$ and subsequently a stronger bond (N1-H1$\cdots$Br2 3.38 Å). We have not explored whether a wider solid solution may exist between [4-MeImH]PbBr$_3$ and [4-MeImH]$_{0.6}$[ImH]$_{0.4}$PbBr$_3$; however it is notable that [4-MeImH]$_{0.6}$[ImH]$_{0.4}$PbBr$_3$ has a slightly higher density than [4-MeImH]PbBr$_3$, suggesting that incorporation of [4-MeImH] results in marginally more efficient packing.

3.2. 2D edge- and face-sharing layers

Similar reactions to those employed in the synthesis of 1 using a 2:2 ratio of [4-MeImH]:PbBr$_2$ were carried out targeting a (110)-oriented perovskite with nominal formula [4-MeImH]$_2$PbBr$_4$, however this proved unsuccessful. Instead, all attempts yielded [4-MeImH]Pb$_2$Br$_5$, a unique 2D layered structure (Fig. 2) consisting of both edge- and face-sharing 7-coordinate Pb polyhedra (Fig. 3). The compound crystallises in the monoclinic space group $P2_1/c$ with Pb-Br bond distances ranging from 2.9511(8) to 3.2822(10) Å. While this is not the first report of a hybrid material containing a 7-coordinate Pb polyhedron,[32–39] we believe that this is the first structure reported that consists solely of 7-coordinate Pb polyhedra rather than as a mixture of other coordination environments, as well as the only example that features exclusively edge- & face-sharing polyhedral connectivity, as shown in Fig. 3. Analysis of the inorganic framework shows two Pb environments, both of which may be regarded as mono-capped trigonal prisms. Equivalent Pb polyhedral environments (Pb1-Pb1 and Pb2-Pb2) are connected through triangular-face-sharing while inequivalent environments (Pb1-Pb2) are connected through edge-sharing involving two distinct pathways, and resulting in the corrugated layer arrangement (Fig. 2). The calculated bond valence sums of each environment indicate that the unusual 7-coordinate structure is readily accommodated and results in bond valence sums comparable with the octahedral Pb environments presented here (V$_{Pb1}$ = 1.91 v.u., V$_{Pb2}$ = 1.87 v.u.). However, by contrast the edge-sharing Br5 shown on the right in Fig. 3(b), between adjacent face-sharing chains is severely 'underbonded' (V$_{Br5}$ = 0.40 v.u.). Inspection of the hydrogen bonding arrangements in [4-MeImH]Pb$_2$Br$_5$ (shown in Fig. 2) show there are no hydrogen bonds formed to stabilise this 'underbonding'. This is likely due to the required spatial positioning of the Me-group into the cavity between layers. This defined arrangement results in a short interlayer distance between adjacent Br4 atoms of ~4.00 Å,

which can be considered as a similar size to the [4-MeImH] moiety. Both N1 and N2 are capable of forming two hydrogen bonds to the other Br atoms present providing stabilisation to the chain portion of the structure.

3.3. Face- and corner-sharing hexagonal perovskite derivatives

Due to the unusual structure of [4-MeImH]Pb_2Br_5, similar reactions utilising a mixture of 4-methylimidazole and imidazole were attempted, aiming to synthesise a mixed cationic species of formula [4-MeImH]$_{1-x}$[ImH]$_x$Pb$_2$Br$_5$. Instead, we obtained a mixture of crystalline products of composition [ImH]PbBr$_3$ and [4-MeImH]$_4$[ImH]$_5$Pb$_6$Br$_{21}$. The first of these, [ImH]PbBr$_3$, adopts a distorted, but conventional, 4H perovskite-like structure (Fig. 4) and crystallises in the orthorhombic space group *Pnma*. The aristotype 4H perovskite structure[40] adopts a hexagonal unit cell, space group *P6$_3$/mmc*, typified by the ambient temperature structures of [DMA]PbCl$_3$ and [DMA]PbBr$_3$.[41] [ImH]PbBr$_3$ has a symmetry-lowering distortion leading to the observed $\sim \sqrt{3}a \times c \times a$ cell metrics relative to the aristotype. This appears to be triggered by the alternating orientations of the imidazolium moiety, coupled to a slight anti-phase rotation of alternating octahedra around the *b*-axis [Fig. 4(a)]. There appear to be only three previously reported hybrid lead halides with the 4H structure (Table 3). Both of the DMA derivatives display sub-ambient temperature phase transitions to a chiral polymorph, space group *P2$_1$2$_1$2$_1$*, with similar unit cell metrics to those in [ImH]PbBr$_3$, but showing much larger distortions (Table 3).

Like [4-MeImH]Pb_2Br_5, [4-MeImH]$_4$[ImH]$_5$Pb$_6$Br$_{21}$ also adopts a very interesting and unique structure. Both [4-MeImH] and [ImH] have been incorporated into the structure resulting in a significantly large and complex unit cell. The compound crystallises in the monoclinic space group *C2/c*, and it consists of face- and corner-sharing octahedra (Fig. 5), with an arrangement based on face-shared dimers similar to the 4H-perovskite structure. A key difference, however, can be seen from the Pb-Br stoichiometry. The fact that this is not 1:3 suggests that the full 3D connectivity is broken somehow, with the introduction of some terminal Pb-Br bonds. Closer inspection reveals the nature of this adaptation. There are three crystallographically distinct octahedral Pb sites, which may be regarded as Pb(1)Br$_{4/2}$Br$_2$, Pb(2)Br$_{6/2}$ and Pb(3)Br$_{5/2}$Br. In other words, Pb(2) shares common bromide ligands with six adjacent octahedra, whereas the Pb(1) octahedron shares only four vertices, with one octahedral edge accommodating two terminal Br ligands; Pb(3) has a single terminal vertex. In turn, two Pb(3)-centred octahedra form a common dimer, whilst a distinct dimer is composed of the Pb(1) and Pb(2)-centred octahedra. The resulting building unit is shown in Fig. 5. These units further link into a complex 2D layered arrangement, with no direct covalent links to neighbouring layers (Fig. 5c). There are nine crystallographically-distinct organic moieties, and we find it is possible to assign these unambiguously to well-ordered [ImH] and [4-MeImH] units. Both [ImH] and [4-MeImH] are capable of forming up to four hydrogen bonds from donor N-H atoms, with N-H···Br distances ranging from 2.55-3.17 Å. Due to the additional steric hindrance of the Me-group in [4-MeImH], this is only located between 2D layers. By comparison, the smaller [ImH] cation can be accommodated in the hexagonal 'channel'-like positions throughout the structure (see Fig S1). A useful comparison of the mean distortion level and bond angle variance in [ImH]PbBr$_3$

and [4-MeImH]$_4$[ImH]$_5$Pb$_6$Br$_{21}$ compared to existing 4H-type lead halides can be made (Table 3). Although the largest bond angle variance values calculated are for [DMA]PbCl$_3$ this is not surprising as large distortion values are common in lead chloride materials. The large Δd values in [4-MeImH]$_4$[ImH]$_5$Pb$_6$Br$_{21}$, particularly Pb1, compared to [ImH]PbBr$_3$ suggest a much larger degree of octahedral distortion than the more typical 4H-perovskite structure observed in [ImH]PbBr$_3$. This may be attributable to the reduction in symmetry due to the incorporation of terminal Pb-Br bonds, and also to the stricter limitation on hydrogen bonding capacity of [4-MeImH] compared to [ImH] arising from the greater degree of steric effects attributable to the Me-group. The difference in hydrogen bonding capability in [ImH]PbBr$_3$ and [4-MeImH]$_4$[ImH]$_5$Pb$_6$Br$_{21}$ is further enhanced by the rotational disorder (around the plane of the molecule) of [ImH] in [ImH]PbBr$_3$ to optimise potential hydrogen bonding. The synthesis of an analogous composition to [4-MeImH]$_4$[ImH]$_5$Pb$_6$Br$_{21}$, utilising the isomeric 1-methylimidazole instead of 4-methylimidazole, was attempted in the hope of probing the impact of further disrupting potential hydrogen bonding while maintaining similar steric hindrance, however only [1-MeImH] was incorporated into the structure resulting in the 2H-perovskite, [1-MeImH]PbBr$_3$ (see ESI for more information).

Although the polyhedral connectivity may differ across the compositions presented, the shortest Br-Br 'interlayer' or 'interchain' distances are relatively similar across all compositions. The shortest of these (4.002(9) Å in [4-MeImH]Pb$_2$Br$_5$) is close to the shortest interlayer distance reported for the corner-linked (110)-oriented perovskite [EPZ-dp]PbBr$_4$ (3.90 Å)[42] and of a similar size to one of the shortest reported for (100)-oriented perovskites, in the n = 3 [3-AMP][MA]Pb$_3$I$_{10}$ structure (3.97 Å)[43], where [EPZ-dp] = 1-ethylpiperazinium; [4-AMP] = 4-(aminomethyl)piperidinium; [MA] = methylammonium.

4. Conclusions

In conclusion, we have prepared several new hybrid organic-inorganic lead bromide materials templated by 4-methylimidazolium. In [4-MeImH]PbBr$_3$ and [4-MeImH]$_{0.6}$[ImH]$_{0.4}$PbBr$_3$ we provide two new examples of an uncommon structure-type consisting of [PbBr$_3$]$_\infty$ edge-sharing chains. In [4-MeImH]Pb$_2$Br$_5$ we present the first example of a two-dimensional layered material containing 7-coordinate Pb and featuring both edge- and face-sharing polyhedra. Finally, both [ImH]PbBr$_3$ and [4-MeImH]$_4$[ImH]$_5$Pb$_6$Br$_{21}$ were prepared from the same reaction and consist of corner- and face-sharing octahedral units related to the 4H-perovskite structure. However, while the former does adopt a fully 3D-connected 4H-perovskite structure, the latter has a much more complex layered structure containing terminal Pb-Br bonds. The versatility of 4-methylimidazolium as a structure-directing agent has resulted in several unusual structures that have not previously been observed, featuring unusual polyhedral connectivity. This work prompts further study of the structure-directing effects of imidazolium derivatives, and other similar disc-shaped amines, in hybrid organic-inorganic materials in the pursuit of new previously unrealised structure-types. Isolation of further examples of the novel layered architectures found in [4-MeImH]Pb$_2$Br$_5$ and [4-MeImH]$_4$[ImH]$_5$Pb$_6$Br$_{21}$, and an understanding of the factors directing their formation would be of particular interest.

Conflicts of interest

There are no conflicts to declare.

Acknowledgements

References

1   M. A. Green, A. Ho-Baillie and H. J. Snaith, The emergence of perovskite solar cells, Nat. Photonics, 8 (2014), 506–514. https://doi.org/10.1038/nphoton.2014.134.

2   S. Brittman, G. W. P. Adhyaksa and E. C. Garnett, The expanding world of hybrid perovskites: materials properties and emerging applications, MRS Commun., 5 (2015), 7–26. https://doi.org/10.1557/mrc.2015.6.

3   B. Saparov and D. B. Mitzi, Organic-inorganic perovskites: structural versatility for funcitonal materials design, Chem. Rev., 116 (2016), 4558–4596. https://doi.org/10.1021/acs.chemrev.5b00715.

4   D. B. Mitzi, Templating and structural engineering in organic-inorganic perovskites, J. Chem. Soc. Dalt. Trans., 2001, 1–12. https://doi.org/10.1039/B007070J.

5   M. Daub, C. Haber and H. Hillebrecht, Synthesis, crystal structures, optical properties, and phase transitions of the layered guanadinium-based hybrid perovskites $[C(NH_2)_3]_2MI_4$; M = Sn, Pb, Eur. J. Inorg. Chem., 2017(2017), 1120–1126. https://doi.org/10.1002/ejic.201601499.

6   M. Szafrański and A. Katrusiak, Phase transitions in the layered structure of diguanidinium tetraiodoplumbate, Phys. Rev. B - Condens. Matter Mater. Phys., 61 (2000), 1026–1035. https://doi.org/10.1103/PhysRevB.61.1026.

7   Y.-Y. Guo, L.-J. Yang, J. A. McNulty, A. M. Z. Slawin and P. Lightfoot, Structural variations in (001)-oriented layered lead halide perovskites, templated by 1,2,4-triazolium, Dalt. Trans., 49 (2020), 17274-17280. https://doi.org/10.1039/D0DT02936J.

8   M. D. Smith, E. J. Crace, A. Jaffe and H. I. Karunadasa, The diversity of layered halide perovskites, Annu. Rev. Mater. Res., 48 (2018), 111–136. https://doi.org/10.1146/annurev-matsci-070317-124406.

9   Y.-Y. Guo, J. A. McNulty, N. A. Mica, I. D. W. Samuel, A. M. Z. Slawin, M. Buhl and P. Lightfoot, Structure-directing effects in (110)-layered hybrid perovskites containing two distinct organic moieties, Chem. Commun., 55 (2019), 9935–9938. https://doi.org/10.1039/C9CC04964A.

10   Y.-Y. Guo, L.-J. Yang, S. Biberger, J. A. McNulty, T. Li, K. Schötz, F. Panzer and P. Lightfoot, Structural diversity in layered hybrid perovskites, A_2PbBr_4 or $AA'PbBr_4$, templated by small disc-shaped amines Inorg. Chem., 59 (2020), 12858-12866. https://doi.org/10.1021/acs.inorgchem.0c01807.

11   J. A. McNulty and P. Lightfoot, Unprecedented tin iodide perovskite-like structures featuring ordering of organic moieties, Chem. Commun., 56 (2020), 4543–4546.

https://doi.org/10.1039/D0CC00549E.

12   J. A. McNulty, A. M. Z. Slawin and P. Lightfoot, Variable dimensionality in 'hollow' hybrid tin iodide perovskites, Dalt. Trans., 49 (2020), 15171–15174. https://doi.org/10.1039/D0DT03449E.

13   M. P. Hautzinger, J. Dai, Y. Ji, Y. Fu, J. Chen, I. A. Guzei, J. C. Wright, Y. Li and S. Jin, Two-dimensional lead halide perovskites templated by a conjugated asymmetric diammonium, Inorg. Chem., 56 (2017), 14991–14998. https://doi.org/10.1021/acs.inorgchem.7b02285.

14   Z. Xiao, Z. Song and Y. Yan, From lead halide perovskites to lead-free metal halide perovskites and perovskite derivatives, Adv. Mater., 2019, 1803792, 1–22. https://doi.org/10.1002/adma.201803792.

15   J. A. McNulty and P. Lightfoot, Structural chemistry of layered lead halide perovskites containing single octahedral layers, IUCrJ., 8 (2021), 485-513. https://doi.org/10.1107/S2052252521005418.

16   J. Tian, D. B. Cordes, C. Quarti, D. Beljonne, A. M. Z. Slawin, E. Zysman-Colman and F. D. Morrison, Stable 6H organic-inorganic hybrid lead perovskite and competitive formation of 6H and 3C perovskite structure with mixed A cations, ACS Appl. Energy Mater., 2 (2019), 5427–5437. https://doi.org/10.1021/acsaem.9b00419.

17   P. Gratia, I. Zimmermann, P. Schouwink, J. H. Yum, J. N. Audinot, K. Sivula, T. Wirtz and M. K. Nazeeruddin, The many faces of mixed ion perovskites: unraveling and understanding the crystallization process, ACS Energy Lett., 2 (2017), 2686–2693. https://doi.org/10.1021/acsenergylett.7b00981.

18   Y.-Y. Guo, L.-J. Yang and P. Lightfoot, Three new lead iodide chain compounds, $APbI_3$, templated by molecular cations, Crystals, 9 (2019), 1–9. https://doi.org/10.3390/cryst9120616

19   G. C. Papavassiliou, G. A. Mousdis, C. P. Raptopoulou and A. Terzis, Preparation and characterization of $[C_6H_5CH_2NH_3]_2PbI_4$, $[C_6H_5CH_2CH_2SC(NH_2)_2]_3PbI_5$ and $[C_{10}H_7CH_2NH_3]PbI_3$ organic-inorganic hybrid compounds, Z. Naturforsch., B 54 (1999), 1405–1409. https://doi.org/10.1515/znb-1999-1112.

20   C. Lermer, S. P. Harm, S. T. Birkhold, J. A. Jaser, C. M. Kutz, P. Mayer, L. Schmidt-Mende and B. V. Lotsch, Benzimidazolium lead halide perovskites: effects of anion substitution and dimensionality on the bandgap, Z. Anorg. Allg. Chem., 642 (2016), 1369–1376. https://doi.org/10.1002/zaac.201600371.

21   A. Samet, S. Triki and Y. Abid, Resonantly enhanced white-light emission involving energy and charge transfer in one-dimensional hybrid material: $(ABT)_2[PbBr_3]$, J. Phys. Chem. C, 123 (2019), 6213–6219. https://doi.org/10.1021/acs.jpcc.9b00361.

22   O. Medhioub, H. Barkaoui, A. Samet, S. Pillet, S. Triki and Y. Abid, Blue emission from charge-transfer excitons in hybrid organic-inorganic quantum wires: $(ABT)[PbCl_3]$, J. Phys. Chem. C., 123 (2019), 26547-26553. https://doi.org/10.1021/acs.jpcc.9b08240.

23   C. Han, D. B. Cordes, A. M. Z. Slawin and P. Lightfoot, Structural variations in manganese halide chain compounds mediated by methylimidazolium isomers, Crystals, 10 (2020), 930. https://doi.org/10.3390/cryst10100930.

24   CrystalClear -SM Expert v2.1. Rigaku Americas, The Woodlands, Texas, USA, and Rigaku Corporation, Tokyo, Japan, 2015.

25   CrysAlisPro v1.171.38.46. Rigaku Oxford Diffraction, Rigaku Corporation, Oxford, U.K., 2015.

26   G. M. Sheldrick, *SHELXT* - Integrated space-group and crystal-structure determination, Acta Crystallogr. Sect. A, 71 (2015), 3-8. https://doi.org/10.1107/S2053273314026370.

27   G. M. Sheldrick, Crystal structure refinement with *SHELXL*, Acta Crystallogr. Sect. C, 71 (2015), 3–8. https://doi.org/10.1107/S2053229614024218.

28   L. J. Farrugia, *WinGX* and *ORTEP* for *Windows*: an update, J. Appl. Crystallogr., 45 (2012), 849–854. https://doi.org/10.1107/S0021889812029111.

29   O. V. Dolomanov, L. J. Bourhis, R. J. Gildea, J. A. K. Howard, H. J. Puschmann, *OLEX2*: a complete structure solution, refinement and analysis program, J. Appl. Crystallogr. 42 (2009), 339-341. https://doi.org/10.1107/S0021889808042726.

30   D. B. Straus, S. Guo and R. J. Cava, Kinetically stable single crystals of perovskite-phase $CsPbI_3$, J. Am. Chem. Soc., 141 (2019), 11435–11439. https://doi.org/10.1021/jacs.9b06055

31   Y. Y. Guo and P. Lightfoot, Structural diversity of lead halide chain compounds, $APbX_3$, templated by isomeric molecular cations, Dalt. Trans., 49 (2020), 12767–12775. https://doi.org/10.1039/D0DT02782K.

32   Z. Liu, W.-T. Yu, X.-T. Tao and M.-H. Jiang, Crystal structure of bis(4-bromoanilinium) tetrachloroplumbate(II), Zeitschrift fur Krist. - New Cryst. Struct., 219 (2004), 303-304.

33   I. Lofving, The crystal structure of $Pb_2Cl_6[NH_3(CH_2)_2NH_3]$, Acta Chem. Scand., 30 (1976), 715. https://doi.org/10.3891/acta.chem.scand.30a-0715.

34   X. Li, T. T. H. Do, A. Granados del Aguila, Y. Huang, W. Chen, Q. Xiong and Q. Zhang, A 3D haloplumbate framework constructed from unprecedented Lindqvist-like highly coordinated $[Pb_6Br_{25}]^{13-}$ nanoclusters with temperature-dependent emission, Chem. An Asian J., 13 (2018), 3185. https://doi.org/10.1002/asia.201801292.

35   G.-E. Wang, G. Xu, M.-S. Wang, L.-Z. Cai, W.-H. Li and G.-C. Guo, Semiconductive 3-D haloplumbate framework hybrids with high color rendering index white-light emission, Chem. Sci., 6 (2015), 7222. https://doi.org/10.1039/C5SC02501J.

36   M.-H. Jung, K. C. Ko and W. R. Lee, Broadband white-light emission from supramolecular piperazinium-based lead halide perovskites linked by hydrogen bonds, Dalt. Trans., 48 (2019), 15074. https://doi.org/10.1039/C9DT03469B.

37   O. Nazarenko, M. R. Kotyrba, M. Wörle, E. Cuervo-Reyes, S. Yakunin and M. V. Kovalenko, Luminescent and photoconductive layered lead halide perovskite compounds comprising mixtures of cesium and guanidinium cations, Inorg. Chem., 56 (2017), 11552–11564. https://doi.org/10.1021/acs.inorgchem.7b01204.

38   D. G. Billing and A. Lemmerer, Inorganic-organic hybrid materials incorporatinf primary cyclic ammonium cations: the lead bromide and chloride series, CrystEngComm, 11 (2009), 1549–1562. https://doi.org/10.1039/B819455F.

39   Y. Peng, L. Li, Z. Wu, S. Wang, X. Liu, Y. Yao and J. Luo, Tailored synthesis of an unprecedented Pb-Mn hetermetallic halide hybrid with enhanced emission, J. Am. Chem. Soc., 141 (2019), 12197. https://doi.org/10.1021/jacs.9b04829.

40   A. Hardy, Structures cristallines de deux varietes allotropiques de manganite de baryum. Nouvelle structure ABO_3. Acta Crystallogr., 15 (1962), 179-181. https://doi.org/10.1107/S0365110X6200047X.

41   A. García-Fernández, E. J. Juarez-Perez, J. M. Bermúdez-García, A. L. Llamas-Saiz, R. Artiaga, J. J. López-Beceiro, M. A. Señarís-Rodríguez, M. Sánchez-Andújar and S. Castro-García,

Hybrid lead halide [(CH$_3$)$_2$NH$_2$]PbX$_3$ (X = Cl$^-$ and Br$^-$) hexagonal perovskites with multiple functional properties, J. Mater. Chem. C, 7 (2019), 10008–10018. https://doi.org/10.1039/C9TC03543E

42   L. Mao, P. Guo, M. Kepenekian, I. Hadar, C. Katan, J. Even, R. D. Schaller, C. C. Stoumpos and M. G. Kanatzidis, Structural diversity in white-light-emitting hybrid lead bromide perovskites, J. Am. Chem. Soc., 140 (2018), 13078–13088. https://doi.org/10.1021/jacs.8b08691.

43   X. Li, W. Ke, B. Traore, P. Guo, I. Hadar, M. Kepenekian, J. Even, C. Katan, C. C. Stoumpos, R. D. Schaller and M. G. Kanatzidis, Two-dimensional Dion-Jacobson hybrid lead iodide perovskites with aromatic diammonium cations, J. Am. Chem. Soc., 141 (2019), 12880-12890. https://doi.org/10.1021/jacs.9b06398.

Table 1 Crystal and structure refinement data for **1-5** at 173 K.

Composition	[4-MeImH]PbBr$_3$	[4-MeImH]$_{0.6}$[ImH]$_{0.4}$PbBr$_3$	[4-MeImH]Pb$_2$Br$_5$	[ImH]PbBr$_3$	[4-MeImH]$_4$[ImH]$_5$Pb$_6$Br$_{21}$
Formula	C$_4$N$_2$H$_7$PbBr$_3$	C$_{3.6}$N$_2$H$_{6.2}$PbBr$_3$	C$_4$N$_2$H$_7$Pb$_2$Br$_5$	C$_3$N$_2$H$_5$PbBr$_3$	C$_{31}$N$_{18}$H$_{53}$Pb$_6$Br$_{21}$
Formula Weight	530.02	524.41	897.03	1881.22	3599.06
Colour/habit	Colourless/prism	Colourless/prism	Colourless/needle	Colourless/prism	Colourless/prism
Crystal size (mm^3)	0.15 × 0.15 × 0.38	0.02 × 0.03 × 0.09	0.01 × 0.01 × 0.24	0.04 × 0.06 × 0.06	0.10 × 0.12 × 0.13
Crystal system	Triclinic	Triclinic	Monoclinic	Orthorhombic	Monoclinic
Space group	$P\overline{1}$	$P\overline{1}$	$P2_1/c$	$Pnma$	$C2/c$
a (Å)	4.4308(3)	4.3643(1)	4.0957(11)	14.2063(6)	29.9994(7)
b (Å)	10.4933(7)	10.8092(3)	15.806(4)	14.9288(5)	15.6666(3)
c (Å)	11.5533(8)	11.3086(3)	21.734(5)	8.8702(3)	16.7313(3)
α (º)	101.66(6)	71.877(3)			
β (º)	94.75(6)	79.508(2)	95.243(7)		91.868(2)
γ (º)	93.579(6)	89.025(2)			
V (Å^3)	522.53(13)	498.09(2)	1401.1(6)	1881.22(12)	7859.3(3)
Z	2	2	4	8	4
Density (g/cm^3)	3.369	3.497	4.253	3.644	3.042
μ (mm^{-1})	27.554	28.904	38.276	30.609	23.521
F(000)	464	458	1536	1792	6368
Measured reflns.	5367	6524	16602	9450	50059
Independent reflns. (R_{int})	2384 (0.0660)	2184 (0.0278)	2555 (0.0634)	2341 (0.0543)	9056 (0.0383)
Goodness of fit	0.984	1.003	0.925	1.185	1.036
R_1 [I >2 σ(I)]	0.0387	0.0230	0.0226	0.0422	0.0273
wR_2 (all data)	0.0930	0.0430	0.0517	0.1169	0.0554
Largest diff. peak/hole (e/Å^3)	2.378/-2.745	0.986/-1.077	1.550/-1.037	3.121/-1.649	1.224/-0.986

Table 2 Summary of calculated bond length distortions (Δd) and bond angle variance (σ^2) for 1D edge-sharing chain compounds reported here and in the literature.

	Δd ($\times 10^{-4}$)	σ^2	BVS			
			Pb	X1	X2	X3
[4-MeImH]PbBr$_3$	25.47	13.54	1.93	0.68	0.56	0.69
[4-MeImH]$_{0.6}$[ImH]$_{0.4}$PbBr$_3$	21.82	4.50	1.96	0.68	0.57	0.72
[4-MeImH]PbI$_3$[19]	17.32	13.88	1.86	0.66	0.50	0.70
[ABT]PbBr$_3$[22] [a]	21.30	10.70	1.82	0.56	0.54	0.71
[Q]PbBr$_3$[32] [b]	9.34	16.66	1.79	0.70	0.40	0.68
δ-CsPbI$_3$[31]	10.61	19.00	2.04	0.69	0.55	0.81

[a][ABT] = 2-aminobenzothiazole; [b][Q] = quinolinium

Figure 1 Views of the crystal structures of (a) δ-CsPbI$_3$ along the *b*- and *a*-axes, (b) [4-MeImH]PbBr$_3$ along the *a*- and *b*-axes and (c) [4-MeImH]$_{0.6}$[ImH]$_{0.4}$PbBr$_3$ along the *a*- and *c*-axes showing the (left) 1D unit-cell packing and (right) edge-sharing [PbX$_3$]$_\infty$ chains. Hydrogen bonding is shown in [4-MeImH]PbBr$_3$ and [4-MeImH]$_{0.6}$[ImH]$_{0.4}$PbBr$_3$ by the red lines. Note that in [4-MeImH]$_{0.6}$[ImH]$_{0.4}$PbBr$_3$ both [4-MeImH] and [ImH] occupy the same

site but only one of each amine is shown for clarity and to show the difference in spatial arrangement.

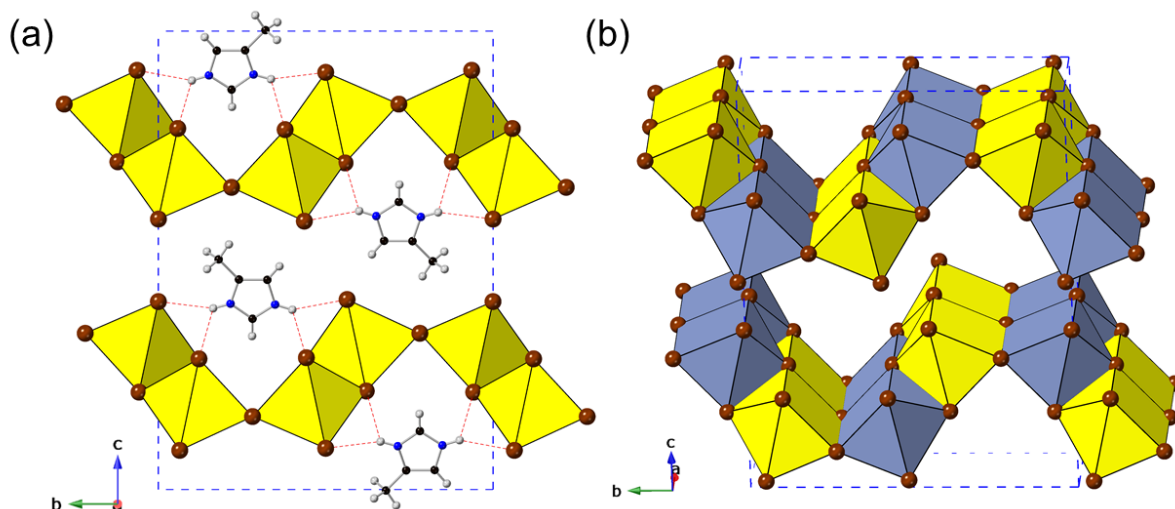**Figure 2** (a) Crystal structure of [4-MeImH]Pb$_2$Br$_5$ viewed along the *a*-axis showing the arrangement of the [4-MeImH] moiety, highlighting hydrogen-bonding. (b) Layer-like 2D structure of [4-MeImH]Pb$_2$Br$_5$ with face-sharing and edge-sharing octahedra. The two different polyhedra are shown in yellow and blue, respectively.
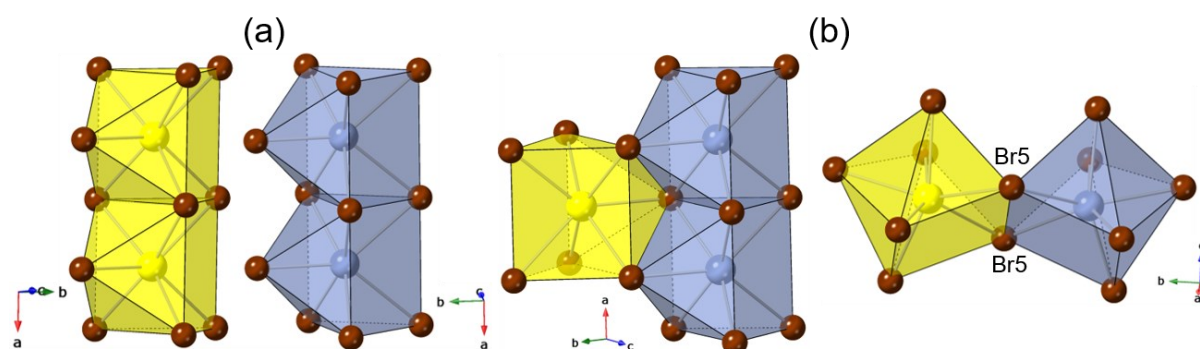

Figure 3 Polyhedral connectivity in [4-MeImH]Pb$_2$Br$_5$. (a) Face-sharing between equivalent Pb1-Pb1 (yellow) and Pb2-Pb2 (blue) polyhedra; (b) Two different edge-sharing arrangements between inequivalent Pb1-Pb2 polyhedra.
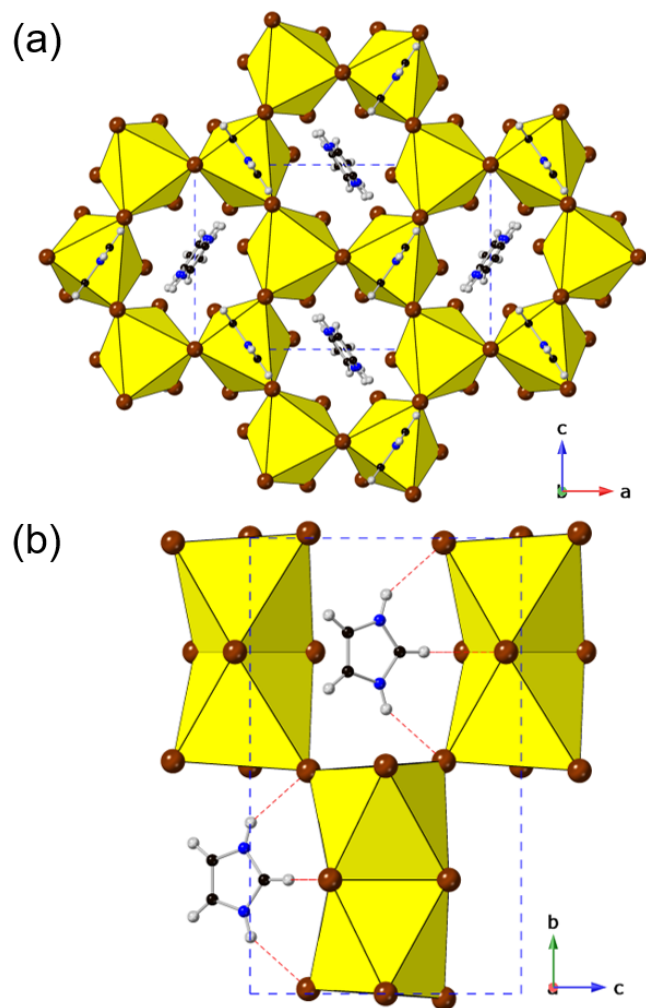
Figure 4 Views of the crystal structure of [ImH]PbBr$_3$ along the (a) *b*- and (b) *a*-axes highlighting the typical 4H-perovskite structural arrangements and possible hydrogen bonding.
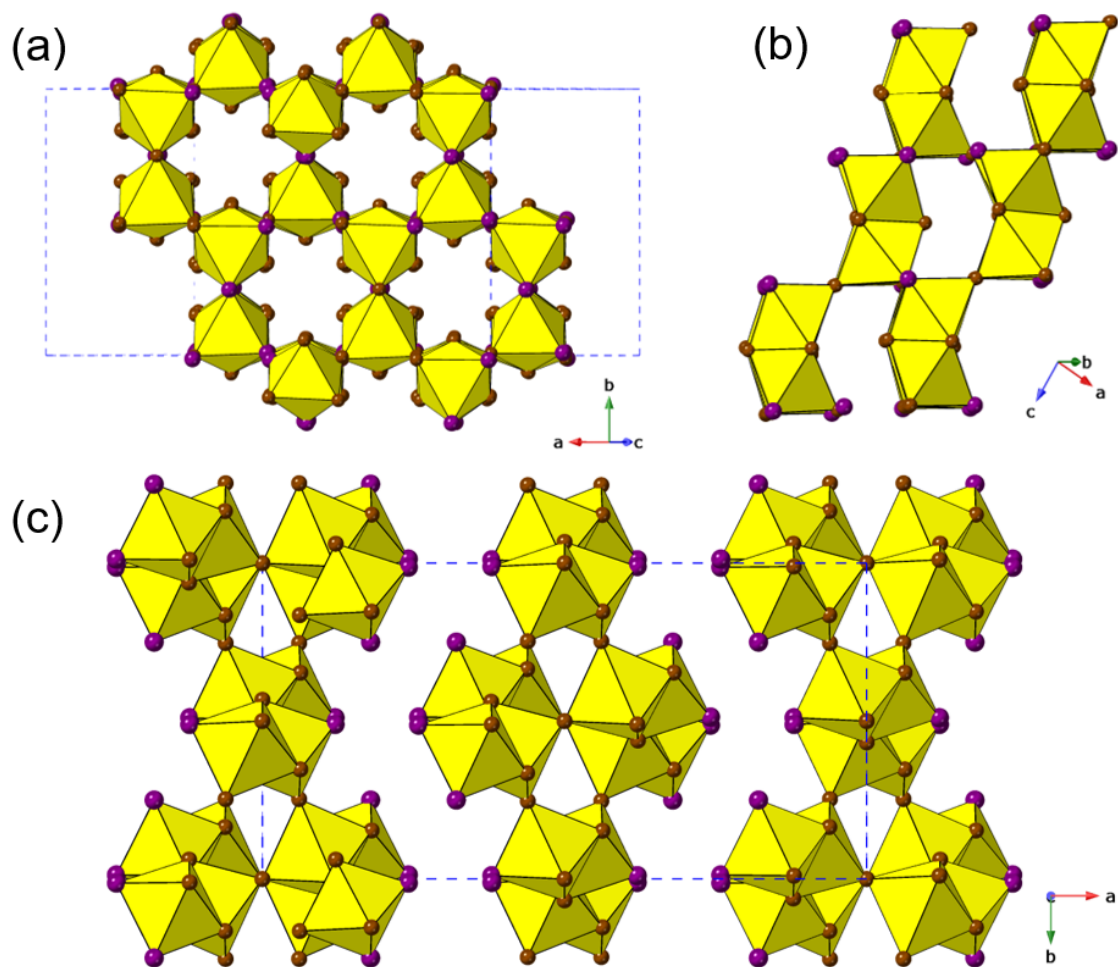
Figure 5 (a) View of a two-dimensional sheet in the crystal structure of [4-MeImH]$_4$[ImH]$_5$Pb$_6$Br$_{21}$. (b) Partial representation of the structure highlighting the presence of both face-sharing and corner-sharing of polyhedra and the resemblance to a 4H-perovskite structure. (c) Complex 2D layered arrangement with no covalent links to neighbouring layers. Note that the amines have been omitted for clarity. Terminal Br ligands are shown as the larger purple spheres.